Morphology-sensitive Trapping States of Photogenerated Charge Carriers on $SrTiO_3$ Particles Studied by Time-resolved Visible to Mid-IR Absorption Spectroscopy: the Effects of Molten Salt Flux Treatments

Akira Yamakata*[1,2], Ham Yeilin[3], Masayuki Kawaguchi[1], Takashi Hisatomi[3], Jun Kubota[3], Yoshihisa Sakata[4], Kazunari Domen*[3]

1. Graduate School of Engineering, Toyota Technological Institute, 2-12-1 Hisakata, Tempaku, Nagoya 468-8511, Japan.
2. Precursory Research for Embryonic Science and Technology (PRESTO), Japan Science and Technology Agency (JST), 4-1-8 Honcho Kawaguchi, Saitama 332-0012, Japan.
3. Department of Chemical System Engineering, the University of Tokyo, 7-3-1 Hongo, Bunkyo-ku, Tokyo 113-8656, Japan.
4. Graduate School of Science and Engineering, Yamaguchi University, 2-16-1 Tokiwadai Ube 755-8611, Japan.

*Corresponding Authors
E-mail address:
yamakata@toyota-ti.ac.jp
domen@chemsys.t.u-tokyo.ac.jp

© 2015. This manuscript version is made available under the Elsevier user license
http://www.elsevier.com/open-access/userlicense/1.0/

Abstract

The effects of the morphology-change of $SrTiO_3$ particles on the behavior of photogenerated charge carriers are studied by time-resolved absorption (TA) spectroscopy from the visible to mid-IR region. In the case of as-purchased defect-rich commercial $SrTiO_3$ particles, most of the charge carriers are deeply trapped, showing a transient absorption peak at 11000 cm^{-1}. Scanning electron microscopy reveals that the irregular-shaped primary particles are heavily aggregated and that the photocatalytic activity for the water splitting reaction is negligibly small. However, when this powder is flux-treated by $SrCl_2$, fine cubic $SrTiO_3$ crystals exposing well-defined surfaces are formed and the photocatalytic activity is greatly improved. TA measurements show that the spectral shape is changed dramatically: the number of deeply trapped electrons is reduced, and that of shallowly trapped electrons producing the absorption band at 2500 cm^{-1} is increased. The change in electron trap depth, observed upon flux treatment, is due to the decrease in the number of defects. We also found that further flux treatment in an Al_2O_3 crucible (i) induces Al doping into $SrTiO_3$, (ii) enhances the photocatalytic activity, (iii) changes the spectral shape, and (iv) prolongs the lifetime of shallowly trapped electrons. The increase in photocatalytic activity is presumably due to the change in lifetime.

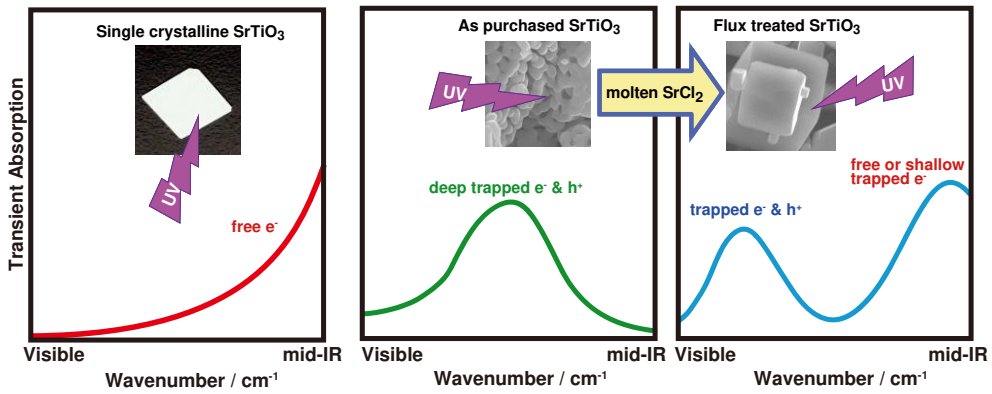

1. Introduction

$SrTiO_3$ is one of the most widely used materials for optical and electronic devices, owing to such properties as a strong dielectric constant, a strong nonlinear optical effect, and ferroelectricity. It is also used as a photocatalyst since it is nontoxic and stable during photocatalytic reactions. [1-4] Furthermore, it turns to a visible-responsive photocatalyst when doped with impurities such as Cr, Ni and Rh: doping induces visible light absorption and promotes photocatalytic reactions. [2-4] For optoelectronic devices, well-defined single crystals are often used, but for photocatalysts, the powder form is preferred since the surface area of a powder is much larger than that of a single crystal. However, there is a disadvantage associated with powders: they are richer in surface defects than single crystals. It is widely believed that these defects capture photogenerated charge carriers and decrease the photocatalytic activity. Therefore, in principle, the number of defects should be reduced in order to increase the photocatalytic activity. Flux treatment is a powerful method that can be used to this end, since dissolution and recrystallization proceed in molten salts. It has been reported that flux treatment of $CaZrTi_2O_7$, [5] Ta_3N_5, [6, 7] $LaTiO_2N$ [8] and $SrTiO_3$ [9] results in well-crystallized particles exposing well-defined surfaces and enhances their photocatalytic activity. Since photocatalytic activity is determined by the behavior of photogenerated charge carriers, the behavior of charge carriers should be elucidated for a precise understanding of the role of flux treatment in activity enhancement.

Time-resolved absorption spectroscopy in the visible to mid-IR region [10, 11] is a powerful method for elucidating the behavior of photogenerated charge carriers, since free electrons [12-20] in the conduction band (CB) give rise to structureless broad absorption in the mid-IR region. Trapped electrons and holes in mid-gap states also give transient absorption peaks in the visible or near-IR (NIR) regions [21-27]; therefore, the energy states of photogenerated charge carriers as well as the decay processes can be examined. We have demonstrated the effectiveness of this method in elucidating the behavior of photogenerated charge carriers in CoO_x-loaded $LaTiO_3$, [10] which is the most efficient photocatalyst for oxidizing water under visible light. We found that the CoO_x cocatalyst captures holes from $LaTiO_2N$ rapidly (within a few ps) and enhances the charge separation of holes and electrons in CoO_x and $LaTiO_2N$, respectively. Furthermore, most of the electrons in $LaTiO_2N$ are deeply trapped in the mid-gap states but the CoO_x cocatalyst decreases the depth of the electron traps. This method was also used to investigate the behavior of charge carriers in powder and single-crystalline $SrTiO_3$. [11] We found that free or shallowly trapped electrons are dominant in single crystals, while most charge carriers are deeply trapped in the case of powder particles. However, the trapped charge carriers in powder particles have longer lifetimes than those in single crystals and still show reactivity toward the reactant molecules. Thus, time-resolved visible to mid-IR absorption spectroscopy is very useful for investigating the behavior of photogenerated charge carriers in semiconductors.

In the present study, we employed time-resolved visible to mid-IR spectroscopy to study the effects of flux treatment on the behavior of photogenerated charge carriers. Defect-rich commercial $SrTiO_3$ powder was used. The powder was flux-treated with molten $SrCl_2$ salt. Changes in the structure and steady-state photocatalytic activity of the $SrTiO_3$ powder were measured, and the behavior of photogenerated charge carriers was investigated.

2. Experimental

Time-resolved absorption measurements were performed with laboratory-built spectrometers as

described in our previous papers. [10, 11, 28] Briefly, in the mid-IR region (6000 to 1000 cm^{-1}), the probe IR light was focused on the sample and the transmitted light was monochromated by the spectrometer. The output IR light was detected by an MCT detector (Kolmar) with an AC-coupled amplifier (Stanford Research Systems; SR560). Temporal profiles of the absorption changes were recorded by a digital oscilloscope. The bandgap of the photocatalysts was excited by 355-nm laser pulses from a Nd:YAG laser (Continuum, Surelite I, 6 ns duration, repetition rate of 10-0.2 Hz). In the visible (25000-10000 cm^{-1}) and near-IR (NIR; 10000-6000 cm^{-1}) regions, the probe light from a halogen lamp (50 W) was focused on the sample, and the diffuse reflected light was monochromated by the spectrometer. The monochromated visible or NIR light was detected by a Si-photodiode or InGaAs detector, respectively. The time resolution of this spectrometer in the NIR and IR regions was 1-2 μs, limited by the time constant of the AC-coupled amplifier, and that in the visible region was ~4 μs, limited by the stray light of the pump pulse and/or short-lived strong emission from the sample.

As-purchased $SrTiO_3$ powder (Wako Pure Chemicals Industries, Ltd., 99.9%) was employed as a raw material without any further treatment. For the flux treatment, $SrTiO_3$ powder and $SrCl_2$ (Kanto Chemicals Co., Inc., 98.0%, anhydrous) were thoroughly mixed in an agate mortar. The mixture was heated in an alumina crucible at 1100°C for 10 h. After the mixture cooled to room temperature, $SrTiO_3$ was separated from the solidified mass by repeated washing with deionized water until no chloride ions were detected by an $AgNO_3$ solution. $SrCl_2$ to $SrTiO_3$ molar ratios of 0.01, 0.1, 1.0, 5.0, 10, and 20 were used; these powders are denoted as FLUX=0.01, 0.1, 1, 5, 10, and 20, respectively.

The crystal structure of the powders was characterized by X-ray diffractometry (XRD; RINT, Rigaku Co.). Specific surface areas were measured with a Belsorp-mini (BEL Japan Inc.). The morphology of the powders was observed using scanning electron microscopy (SEM; S-4700, Hitachi High-Technologies Co.). The photocatalytic activity of the synthesized materials was tested after loading $Rh_xCr_{2-x}O_3$ cocatalysts by the impregnation method. [29] The rate of H_2 and O_2 evolution from water were measured in a closed gas circulation system with a top-irradiation-type reactor. The deionized water (100 mL) was evacuated to remove air completely. The reactor was irradiated using a 300-W xenon lamp ($\lambda > 300$ nm). The evolved gases were analyzed by a gas chromatograph (Shimadzu, GC-8A) equipped with a thermal conductivity detector, using Ar as the carrier gas. The apparent quantum efficiency was measured using a top-irradiation-type reactor with a quartz window. The photocatalyst powder (0.1 g) was dispersed in deionized water (150 mL), and a high-pressure mercury lamp attached with a band pass filter ($\lambda = 350$ nm) was used to illuminate monochromatic light. The number of incident photons was measured by a photodiode, and the number of reacted electrons was determined from the amount of evolved H_2.

For elemental analysis, inductively coupled plasma optical emission spectroscopy (ICP-OES; Shimazu Co., ICPS-8100) was used. STO powder (0.01 g) was melted together with 1.0 g of 3:1 mixture of Na_2CO_3 and $B(OH)_3$ by heating. Aqueous solution of Tartaric acid (5%, 10 mL), HCl (20%, 4 mL), and H_2O_2 (30 wt%, 1 mL) were further added to dissolve the melt, and diluted with distilled water to make the total volume of 100 mL. The obtained solution was used to measure Al and Y. The solution was further diluted 10 fold to measure Sr and Ti.

3. Results and Discussion

3.1 Morphology change in $SrTiO_3$ particles upon $SrCl_2$ flux treatment

Figure 1A shows an SEM image of the $SrTiO_3$ powder as purchased from Wako Chemicals. Clearly, the

crystal shape is not fine: many irregular-shaped primary particles smaller than 1 μm have formed agglomerates larger than 10 μm. When this powder is flux-treated with $SrCl_2/SrTiO_3$=0.01 (FLUX=0.01), the primary particles take on a cubic shape, however, they remain aggregated. The addition of further $SrCl_2$ to $SrCl_2/SrTiO_3$=0.1 promotes recrystallization, resulting in the formation of isolated particles. In Figure 1C, the primary particles observed in Figure 1A have disappeared completely, and new crystals have formed with particle sizes ranging from the submicron range to ~10 μm. Thus, they are still relatively coarse. At $SrCl_2/SrTiO_3$=1 (FLUX=1), the morphologies of the $SrTiO_3$ crystals are further changed: fine cubic crystals exposing well-defined surfaces have formed with a size of a few microns, as shown in Figure 1D. The addition of flux beyond FLUX=1 does not result in a further improvement in the crystal structure: as seen in Figures 1E and 1F, the shape of the $SrTiO_3$ crystals is comparable to that for FLUX=1. These results show that the flux treatment improves the crystal structure of $SrTiO_3$, but a $SrCl_2/SrTiO_3$ ratio of 1 is sufficient for fine recrystallization.

The change in particle shape induced by the flux treatment was also studied by XRD measurements, as shown in Figure 2. Upon flux treatment, the intensities of the diffraction peaks increased, while their widths decreased, as seen in Table 1: the full width at half maximum (FWHM) of the (110) peak was 0.107 for as-purchased sample and 0.058 for FLUX=0.1. This provides further confirmation that the crystallinity improved upon flux treatment.

3.2 Enhancement of photocatalytic activity of $SrTiO_3$ particles by $SrCl_2$ flux treatment

The photocatalytic activity for H_2 and O_2 evolution during water splitting reactions was investigated under UV light irradiation. The results obtained are tabulated in Table 1. In the case of the as-purchased sample, the photocatalytic activity was almost negligible: the rates of H_2 and O_2 evolution were both less than 1 μmol h^{-1}. However, upon flux treatment, the photocatalytic activity for H_2 evolution gradually increased from 1 to 400 μmol h^{-1}. The increase was monotonic between FLUX=0.01 and FLUX=5. The activity was not any higher at FLUX=10, and the highest apparent quantum efficiency was estimated to be 30% under irradiation of 350 nm light.

The increase in photocatalytic activity was presumably due to the change in the morphology of the $SrTiO_3$ particles. However, as shown in Table 1, Al is doped into $SrTiO_3$ during the flux treatment from the Al_2O_3 crucible. Takata et al. have reported that substitution of Ti^{4+} with lower-valence cations such as Ga^{3+} enhances the photocatalytic activity. [30] Since Al is doped as Al^{3+}, it should also promote the photocatalytic activity (we will publish the results studying the detailed effects of Al-doping in other paper). Thus, the morphology change and Al doping of $SrTiO_3$ presumably both contribute to the enhancement of photocatalytic activity.

3.3 Behavior of photogenerated charge carriers in as-purchased commercial $SrTiO_3$ particles

In order to determine the effects of flux treatment on photocatalytic activity, we need to study how the morphology change and Al-doping affect the behavior of photogenerated charge carriers. Thus, we performed time-resolved absorption measurements on the flux-treated $SrTiO_3$. Figure 3A shows the transient absorption spectra of as-purchased $SrTiO_3$ particles. A clear absorption peak is observed around 11000 cm^{-1}. The spectral shape is totally different from that for other commercial $SrTiO_3$ powders purchased from Aldrich and Kojindo Co., which are already reported in our previous paper [11]. In the case of Aldrich and Kojindo powders, three peaks appear at 20000, 11000 and 2500 cm^{-1}, which are assigned to trapped holes, trapped electrons, and shallowly trapped electrons, respectively. However, in the case of the Wako Pure Chemicals powder, the absorption

intensities around 20000 and 2500 cm^{-1} are very small. This suggests that the energy states of the photogenerated charge carriers are completely different, which should be ascribed to the difference in the structure and the property of the defects on the purchased powders.

The cause of the transient absorption is investigated by observing the decay processes of the transient absorption in the presence and absence of electron- and hole-consuming reagents, O_2 gas and MeOH vapor, respectively. Figure 4 shows the decay curves of the transient absorption at 2500, 11000, and 20000 cm^{-1} for as purchased sample. The intensity change at 2500 cm^{-1} shows that the decay is accelerated by exposure to O_2 and decelerated by exposure to MeOH. Since O_2 [13] and MeOH [16] consume electrons and holes, respectively, as reported in our previous papers, this result suggests that the intensity at 2500 cm^{-1} reflects the number of electrons. At 20000 cm^{-1} (Figure 4C), the decay is decelerated by the exposure to O_2. This suggests that the intensity at 20000 cm^{-1} mainly reflects the number of holes. However, the exposure to MeOH did not accelerate the decay. We consider the trapped holes giving the transient absorption at 20000 cm^{-1} are less reactive with MeOH. More reactive free or shallowly trapped holes should be present in the catalysts, but it may not give transient absorption in the range from visible to mid-IR. As demonstrated in our previous work [11], no signal derived from free or shallowly trapped holes is observed in the defect free single-crystal $SrTiO_3$.

By contrast, the intensity at 11000 cm^{-1} reveals complex changes: as shown in Figure 4B, exposure to MeOH vapor and exposure to O_2 both decelerated the transient decay. This suggests that the band intensity at 11000 cm^{-1} involves contributions from both photogenerated electrons and holes. This result can be explained as follows: the hole-consuming reaction decreases the number of holes but increases the number of surviving electrons, and vice versa. Numerical simulation [13] is useful to understand these phenomena, therefore the decay curves of the number of electrons and holes are calculated based on a simple model. As discussed in our previous papers [10, 12-14], the decay of carriers in microsecond regions follow the first-order law, suggesting that the number of electron-hole pair is less than one pair per one particle. In this case, the recombination is represented as follows, [13]

$$e-h \xrightarrow{k_1} h\nu \text{ and/or } \Delta \qquad (1)$$

where e-h is the electron-hole pair in $SrTiO_3$ particles, and k_1 is the rate constant of recombination. On the other hand, the electron- and hole-consuming reactions by adsorbed O_2 and methoxy species (MeO^-) derived from adsorbed MeOH are represented as follows,

$$e-h+O_2(a) \xrightarrow{k_2} h_s^+ + O_2^-(a) \quad \text{and} \quad e_s^- + O_2(a) \xrightarrow{k_2} O_2^-(a) \qquad (2)$$

$$e-h+MeO^-(a) \xrightarrow{k_3} e_s^- + MeO^{\bullet}(a) \quad \text{and} \quad h_s^+ + MeO^-(a) \xrightarrow{k_3} MeO^{\bullet}(a) \qquad (3)$$

where k_2 and k_3 are the rate constants, e_s and h_s represent the separated electron and hole from electron-hole pair in the $SrTiO_3$ particles, respectively. When $k_2[O_2]$ and $k_3[MeO]$ are replaced by k_2' and k_3', the rate equations are described as follows,

$$\frac{d[e-h]}{dt} = -(k_1 + k_2' + k_3')[e-h] \qquad (4)$$

$$\frac{d[e_s]}{dt} = k_3'[e-h] - k_2'[e_s] \qquad (5)$$

$$\frac{d[h_s]}{dt} = k_2'[e\text{-}h] - k_3'[h_s] \quad (6)$$

For the simplicity of the model, we assumed the single component of recombination and initial values at time 0 were set to [e-h]=1, [e_s]=[h_s]=0. The decay curves in a vacuum were calculated by setting the rate constants to k_1=0.01, k_2'=k_3'=0. In the presence of O_2, k_2' was changed to 0.00005. The calculated [e^-]=[e-h]+[e_s], [h^+]=[e-h]+[h_s], and the sum of [e^-] and [h^+] are shown in Figure 5. It is clearly shown that the decay of electrons is accelerated by the reaction with O_2, but that of holes is decelerated. As a result, the decay of the sum of [e^-] and [h^+] is slowed down by the exposure to O_2 compared to that in a vacuum. Essentially, the same results are obtained for MeOH, by setting the parameters to k_2'=0 and k_3'=0.00005. These results confirm us that either the electron- or hole-consuming reaction increases the number of sum of surviving electrons and holes, when the charge-consuming reactions proceed during the recombination. This is that observed in Figure 4B

We have reported in our previous paper [11] that the absorption intensity around 11000 cm^{-1} is very sensitive to the defect structure: in the case of the Aldrich powder this absorption intensity mainly reflects the number of electrons, whereas it reflects mainly holes in the case of the Kojundo powder. These results indicate that the defects on Wako powder that give transient absorption at 11000 cm^{-1} have mixed properties with respect to those of Aldlich and Kojundo, although the detailed structure of the defects are still unknown.

3.4 Behavior of photogenerated charge carriers on flux-treated fine $SrTiO_3$ particles: effects of morphology change

When as-purchased $SrTiO_3$ powders are flux-treated with $SrCl_2$, the spectral shape changed dramatically, as shown in Figures 3B-E. The peak intensity at 11000 cm^{-1} decreased slightly for FLUX=0.01 (Figure 3B), disappearing almost completely for FLUX=0.1 (Figure 3C). Interestingly, new peaks appeared at 20000 and 2500 cm^{-1} with a cut-off at around 2000 cm^{-1}. It looks like the peak at 11000 cm^{-1} was split into two bands at 20000 and 2500 cm^{-1}. Upon further addition of flux to $SrCl_2/SrTiO_3$=1 (Figure 3D), the intensities at 20000 and 2500 cm^{-1} increased further. As discussed in Section 3.1, the shape of the $SrTiO_3$ particles was greatly improved from irregular to fine-cubic shape by increasing the amount of mixed flux from $SrCl_2/SrTiO_3$=0.01 to 1: the particle agglomerates broke up, and fine cubic crystals were formed. The Al concentration increased upon flux treatment; however, the concentration of doped Al remained constant at ~0.2% between $SrCl_2/SrTiO_3$=0.01 and 1. Thus, the abrupt change in the transient spectra between FLUX=0.01 and FLUX=1 is presumably mainly attributable to the morphological change of the $SrTiO_3$ particles.

The cause of the transient absorption is investigated by observing the intensity change in the presence and absence of electron- and hole-consuming reagents. Figure 6 shows the decay curves for the transient absorption at 2500, 11000, and 20000 cm^{-1} on FLUX=1. In the case of the band intensity at 2500 cm^{-1}, the absorption is ascribed to shallowly trapped electrons, since it decreases and increases upon exposure to O_2 and MeOH, respectively. The depth of the electron trap is estimated to be ~0.24 eV from the low-frequency cut-off wavenumber located at around 2000 cm^{-1} (0.24 eV), which is shallower than that estimated from the position of the peak located at 2500 cm-1 (0.31 eV). As for the absorption at 11000 and 20000 cm^{-1}, the intensity also increases and decreases upon exposure to O_2 and MeOH, respectively. These results suggest that the absorption at 20000 and 11000 cm^{-1} mainly reflect the number of trapped electrons. We note that these charge carriers are trapped in the defects, but they still show reactivity toward the reactant molecules.

3.5 Behavior of photogenerated charge carriers on flux-treated fine $SrTiO_3$ particles: effects of Al doping

Further increase of the mixed flux to $SrCl_2/SrTiO_3$=10 induced a dramatic change in the shape of transient absorption spectra (Figure 3E): the band intensities at 20000 and 2500 cm^{-1} increased further. However, the peak at 11000 cm^{-1}, which was present in the as-purchased sample (Figure 3A) but had disappeared upon flux treatment (FLUX=0.1 and FLUX=1, Figures 3C and D), reappeared. SEM and XRD analysis revealed that there was no large difference in crystal structure between FLUX=1 and FLUX=10. Therefore, the reappearance of the 11000-cm^{-1} peak could not be due to a change in morphology of the crystal. As shown in Table 1, the concentration of doped Al increases to 0.31% when the mixed flux increases to $SrCl_2/SrTiO_3$=10. Thus, the appearance of the 11000-cm^{-1} band is presumably attributable to the Al doping.

The decay processes for the transient absorption at 20000, 11000, and 2500 cm^{-1} are further investigated in the presence and absence of reactant gases (Figure 7). In the case of the absorption at 2500 cm^{-1}, the decay is slightly accelerated and decelerated upon exposure to O_2 and MeOH, respectively. However, the change is not as large as in the case of as purchased sample and FLUX=1. On the other hand, the band intensities at 20000 and 11000 cm^{-1} are changed little by exposure to O_2 or MeOH, presumably due to the lower adsorption of these molecules on the surface. It is reported that O_2 [31] and MeOH [32, 33] prefer to adsorb on surface defects, so very little adsorption occurs on the fine crystal surfaces: it is widely believed that surface defects work as reaction centers for chemical reactions [31-33].

The decay curves for the shallowly trapped electrons on the flux-treated $SrTiO_3$ are plotted in Figure 8A. It is clearly seen that the lifetime of electrons observed at 2500 cm^{-1} was prolonged by the flux treatment in going from as purchased to FLUX=10. This trend is well correlated with that for the steady-state photocatalytic activity, as shown in Table 1. In contrast, the decay curves for the deeply trapped electrons and holes, which gave a transient absorption at 20000 and 11000 cm^{-1}, are much more complex (Figure 8B and C): it looks like there is no correlation with the steady-state photocatalytic activity, indicating that the deeply trapped carriers are less reactive with water. As discussed in previous sections, both electrons and holes can show a transient absorption in the visible to NIR region. Therefore, it is very difficult to distinguish the contribution from electrons and holes. However, it should be noted here that the transient absorption in the visible to NIR region is absent in defect-free single-crystalline $SrTiO_3$ [11] and is very sensitive to the structure of defects and impurities. The present study demonstrates that the spectral shape changes dramatically upon flux treatment. We believe that a detailed analysis of the transient absorption in the visible to mid-IR region would enable a fuller understanding of photogenerated charge carriers associated with defects. We cannot remove defects and impurities from powder particles; therefore, a thorough understanding of the behavior of photogenerated charge carriers at defects and impurities is essential for the development of highly active photocatalysts.

4. Conclusion

In this work, we performed time-resolved visible to mid-IR absorption spectroscopy to investigate the effects of flux treatment on the behavior of photogenerated charge carriers in $SrTiO_3$ particles. In the case of the as-purchased sample, most of the charge carriers generated by bandgap excitation were deeply trapped at defects. The depth of the trapped states depended on the defect structure, i.e., the shape of the transient absorption spectrum was totally dependent on the company from which the powder was purchased. When commercial $SrTiO_3$

powders were flux-treated with molten $SrCl_2$, the number of defects was much reduced and fine cubic crystals were formed. In the flux-treated sample, the number of deeply trapped charge carriers was reduced while that of shallowly trapped electrons was increased. We also found that further flux treatment in an Al_2O_3 crucible induced Al doping into $SrTiO_3$ and led to further changes in the transient absorption spectra: a new peak appeared as a result of the Al doping, and the lifetime of shallowly trapped electrons was prolonged.

Acknowledgements

This work was supported by the PRESTO/JST program "Chemical Conversion of Light Energy". The authors would also like to acknowledge the Grant-in-Aid for Specially Promoted Research (No. 23000009) and Basic Research (B) (No. 23360360) of the Ministry of Education, Culture, Sports, Science, and Technology (MEXT) of Japan. One of the authors (A.Y.) thanks the Nippon Sheet Glass Foundation and Nagai Foundation for Science and Technology.

References

[1] K. Domen, S. Naito, M. Soma, T. Onishi, K. Tamaru, Photocatalytic Decomposition of Water-Vapor on an NiO-SrTiO3 Catalyst, J. Chem. Soc.-Chem. Commun. (1980) 543-544.

[2] A. Kudo, Y. Miseki, Heterogeneous Photocatalyst Materials for Water Splitting, Chem. Soc. Rev. 38 (2009) 253-278.

[3] H. Kato, A. Kudo, Visible-light-response and photocatalytic activities of TiO2 and SrTiO3 photocatalysts codoped with antimony and chromium, J. Phys. Chem. B 106 (2002) 5029-5034.

[4] K. Furuhashi, Q. Jia, A. Kudo, H. Onishi, Time-Resolved Infrared Absorption Study of SrTiO3 Photocatalysts Codoped with Rhodium and Antimony, J. Phys. Chem. C 117 (2013) 19101.

[5] Y. Miseki, K. Saito, A. Kudo, Nanocrystalline CaZrTi2O7 Photocatalyst Prepared by a Polymerizable Complex Method in the Presence of Cs2CO3 Flux for Water Splitting, Chem. Lett. 38 (2009) 180-181.

[6] T. Takata, D.L. Lu, K. Domen, Synthesis of Structurally Defined Ta3N5 Particles by Flux-Assisted Nitridation, Cryst. Growth Des. 11 (2011) 33-38.

[7] S.S.K. Ma, T. Hisatomi, K. Maeda, Y. Moriya, K. Domen, Enhanced Water Oxidation on Ta3N5 Photocatalysts by Modification with Alkaline Metal Salts, J. Am. Chem. Soc. 134 (2012) 19993-19996.

[8] F.X. Zhang, A. Yamakata, K. Maeda, Y. Moriya, T. Takata, J. Kubota, K. Teshima, S. Oishi, K. Domen, Cobalt-Modified Porous Single-Crystalline LaTiO2N for Highly Efficient Water Oxidation under Visible Light, J. Am. Chem. Soc. 134 (2012) 8348-8351.

[9] H. Kato, M. Kobayashi, M. Hara, M. Kakihana, Fabrication of SrTiO3 exposing characteristic facets using molten salt flux and improvement of photocatalytic activity for water splitting, Catal. Sci. Technol. 3 (2013) 1733-1738.

[10] A. Yamakata, M. Kawaguchi, N. Nishimura, T. Minegishi, J. Kubota, K. Domen, Behavior and Energy States of Photogenerated Charge Carriers on Pt- or CoOx-loaded LaTiO2N Photocatalysts: Time-resolved Visible to mid-IR Absorption Study, J. Phys. Chem. C 118 (2014) 23897.

[11] A. Yamakata, J. Vequizo, M. Kawaguchi, Behavior and Energy State of Photogenerated Charge Carriers in Single-crystalline and Polycrystalline Powder SrTiO3 Studied by Time-resolved Absorption Spectroscopy in the Visible to mid-Infrared Region, J. Phys. Chem. C 119 (2015) 1880–1885.

[12] A. Yamakata, T. Ishibashi, H. Onishi, Time-Resolved Infrared Absorption Spectroscopy of Photogenerated Electrons in Platinized TiO2 Particles, Chem. Phys. Lett. 333 (2001) 271-277.

[13] A. Yamakata, T. Ishibashi, H. Onishi, Water- and Oxygen-Induced Decay Kinetics of Photogenerated Electrons in TiO2 and Pt/TiO2: A Time-Resolved Infrared Absorption Study, J. Phys. Chem. B 105 (2001) 7258-7262.

[14] A. Yamakata, T. Ishibashi, H. Kato, A. Kudo, H. Onishi, Photodynamics of NaTaO3 Catalysts for Efficient Water Splitting, J. Phys. Chem. B 107 (2003) 14383-14387.

[15] A. Yamakata, M. Yoshida, J. Kubota, M. Osawa, K. Domen, Potential-Dependent Recombination Kinetics of Photogenerated Electrons in n- and p-Type GaN Photoelectrodes Studied by Time-Resolved IR Absorption Spectroscopy, J. Am. Chem. Soc. 133 (2011) 11351-11357.

[16] A. Yamakata, T. Ishibashi, H. Onishi, Electron- and Hole-Capture Reactions on Pt/TiO2 Photocatalyst Exposed to Methanol Vapor Studied with Time-Resolved Infrared Absorption Spectroscopy, J. Phys. Chem. B 106 (2002) 9122-9125.

[17] A. Yamakata, T. Ishibashi, H. Onishi, Effects of water addition on the methanol oxidation on Pt/TiO2 photocatalyst studied by time-resolved infrared absorption spectroscopy, J. Phys. Chem. B 107 (2003) 9820-9823.

[18] A. Yamakata, T. Ishibashi, H. Onishi, Microsecond Kinetics of Photocatalytic Oxidation on Pt/TiO2 Traced by Vibrational Spectroscopy, Chem. Phys. Lett. 376 (2003) 576-580.

[19] A. Yamakata, T. Ishibashi, H. Onishi, Effects of accumulated electrons on the decay kinetics of photogenerated electrons in Pt/TiO2 photocatalyst studied by time-resolved infrared absorption spectroscopy, Journal of Photochemistry and Photobiology a-Chemistry 160 (2003) 33-36.

[20] T. Chen, Z.H. Feng, G.P. Wu, J.Y. Shi, G.J. Ma, P.L. Ying, C. Li, Mechanistic studies of photocatalytic reaction of methanol for hydrogen production on Pt/TiO2 by in situ Fourier transform IR and time-resolved IR spectroscopy, J. Phys. Chem. C 111 (2007) 8005-8014.

[21] B.H. Meekins, P.V. Kamat, Role of Water Oxidation Catalyst IrO2 in Shuttling Photogenerated Holes Across TiO2 Interface, J. Phys. Chem. Lett. 2 (2011) 2304-2310.

[22] D. Bahnemann, A. Henglein, J. Lilie, L. Spanhel, Flash-Photolysis Observation of The Absorption-Spectra of Trapped Positive Holes and Electrons in Colloidal TiO2, J. Phys. Chem. 88 (1984) 709-711.

[23] D.W. Bahnemann, M. Hilgendorff, R. Memming, Charge carrier dynamics at TiO2 particles: Reactivity of free and trapped holes, J. Phys. Chem. B 101 (1997) 4265-4275.

[24] T. Yoshihara, R. Katoh, A. Furube, Y. Tamaki, M. Murai, K. Hara, S. Murata, H. Arakawa, M. Tachiya, Identification of Reactive Species in Photoexcited Nanocrystalline TiO2 Films by Wide-wavelength-Range (400-2500 nm) Transient Absorption Spectroscopy, J. Phys. Chem. B 108 (2004) 3817-3823.

[25] Y. Tamaki, A. Furube, M. Murai, K. Hara, R. Katoh, M. Tachiya, Direct observation of reactive trapped holes in TiO2 undergoing photocatalytic oxidation of adsorbed alcohols: Evaluation of the reaction rates and yields, J. Am. Chem. Soc. 128 (2006) 416-417.

[26] M. Barroso, A.J. Cowan, S.R. Pendlebury, M. Gratzel, D.R. Klug, J.R. Durrant, The Role of Cobalt Phosphate in Enhancing the Photocatalytic Activity of alpha-Fe2O3 toward Water Oxidation, J. Am. Chem. Soc. 133 (2011) 14868-14871.

[27] M. Barroso, C.A. Mesa, S.R. Pendlebury, A.J. Cowan, T. Hisatomi, K. Sivula, M. Gratzel, D.R. Klug, J.R. Durrant, Dynamics of Photogenerated Holes in Surface Modified Alpha-Fe2O3 Photoanodes for Solar Water Splitting, Proc. Natl. Acad. Sci. U. S. A. 109 (2012) 15640-15645.

[28] A. Yamakata, E. Soeta, T. Ishiyama, M. Osawa, A. Morita, Real-Time Observation of the Destruction of Hydration Shells under Electrochemical Force, J. Am. Chem. Soc. 135 (2013) 15033-15039.

[29] K. Maeda, K. Teramura, H. Masuda, T. Takata, N. Saito, Y. Inoue, K. Domen, Efficient overall water splitting under visible-light irradiation on (Ga1-xZnx)(N1-xOx) dispersed with Rh-Cr mixed-oxide nanoparticles: Effect of reaction conditions on photocatalytic activity, J. Phys. Chem. B 110 (2006) 13107-13112.

[30] T. Takata, K. Domen, Defect Engineering of Photocatalysts by Doping of Aliovalent Metal Cations for Efficient Water Splitting, J. Phys. Chem. C 113 (2009) 19386-19388.

[31] H. Tanaka, T. Matsumoto, T. Kawai, S. Kawai, Interaction of oxygen vacancies with O2 on a reduced SrTiO3(100)root-5x-root-5-R26.6-degrees surface observed by STM, Surf. Sci. 318 (1994) 29-38.

[32] T. Yoshikawa, M. Bowker, Reductive coupling desorption of methanol on reduced SrTiO3(110), Phys. Chem. Chem. Phys. 1 (1999) 913-920.

[33] L.Q. Wang, K.F. Ferris, S. Azad, M.H. Engelhard, Adsorption and reaction of methanol on stoichiometric and defective SrTiO3(100) surfaces, J. Phys. Chem. B 109 (2005) 4507-4513.

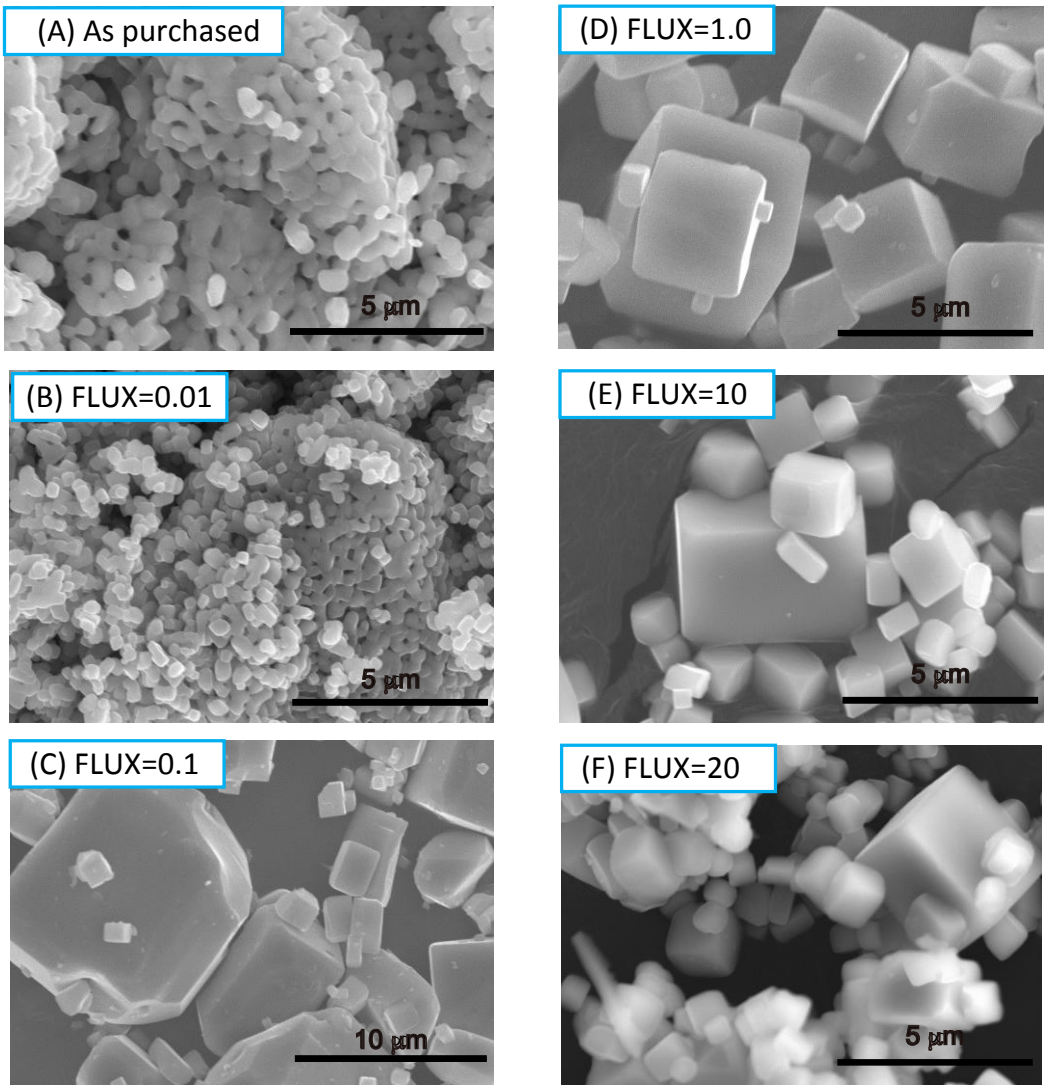

Fig. 1 SEM images of flux-treated $SrTiO_3$ particles. The amount of flux was varied from $SrCl_2/SrTiO_3$=0.01 to 20, and these samples are denoted as FLUX=0.01 to 20.

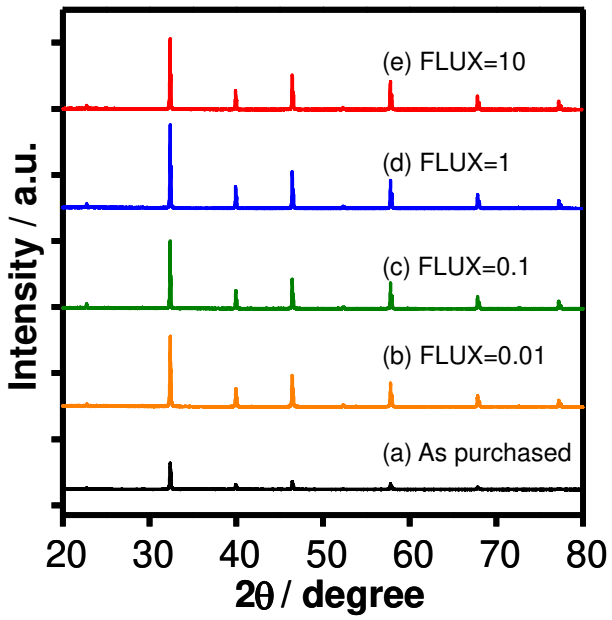

Fig. 2 XRD patterns of flux-treated $SrTiO_3$ particles. The amount of flux was varied from $SrCl_2/SrTiO_3$=0.-1 to 20 (FLUX=0.01 to 20).

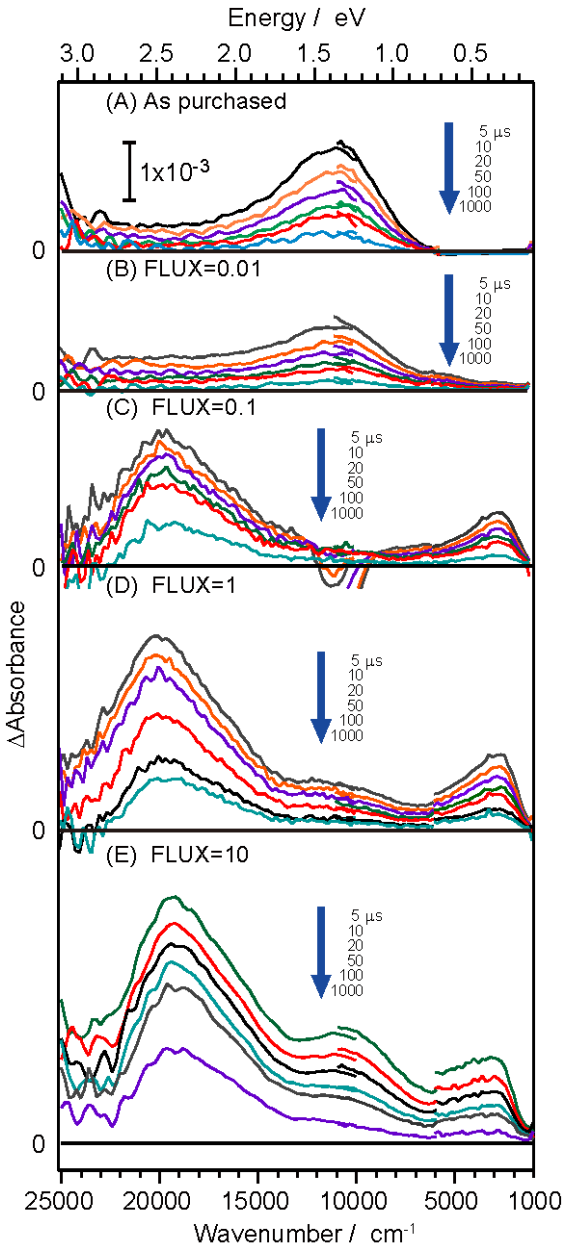

Fig. 3 Transient absorption spectra of flux-treated $SrTiO_3$ particles irradiated by UV (355 nm) laser pulses under vacuum. The pump energy was 0.5 mJ per pulse, and the repetition rate was 5 Hz. The amount of flux was varied from $SrCl_2/SrTiO_3$=0.01 to 20 (FLUX=0.01 to 20).

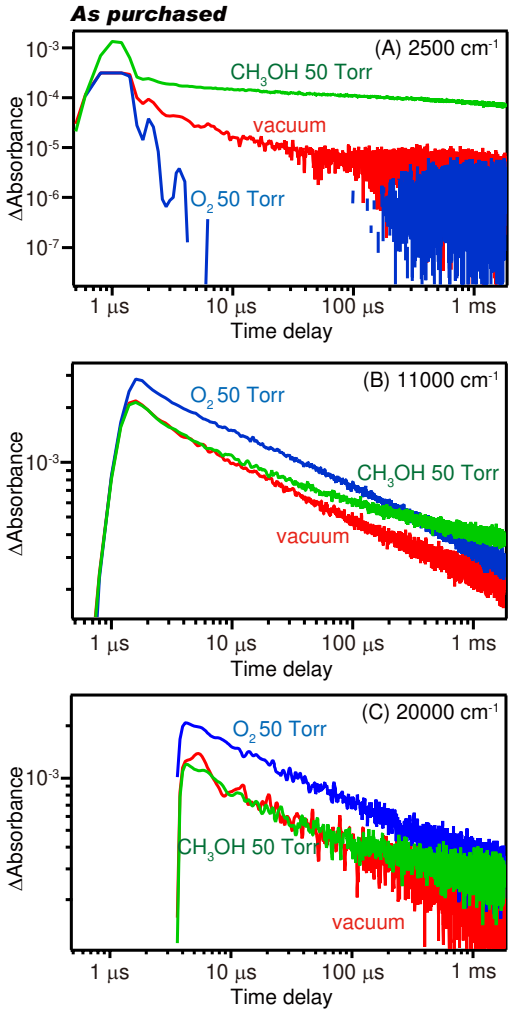

Fig. 4 Decay curves of transient absorption of as-purchased $SrTiO_3$ powder irradiated by 355 nm laser pulses (0.5 mJ per pulse at 0.2 Hz). The decay curves were measured at 2500 cm^{-1} (A), 11000 cm^{-1} (B), and 20000 cm^{-1} (C), in vacuum, 50 Torr O_2, and CH_3OH.

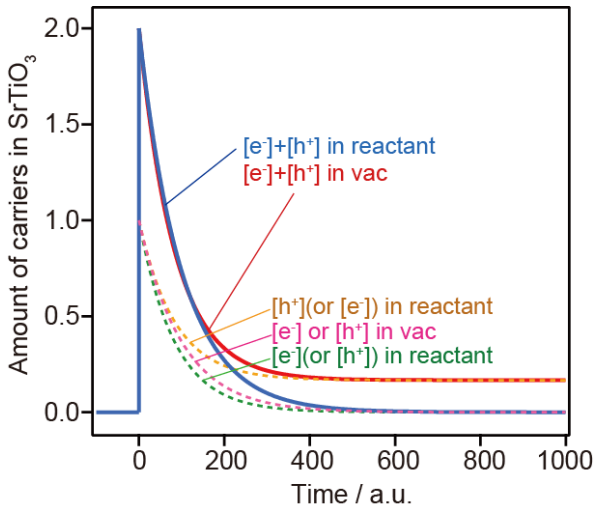

Fig. 5 Numerically simulated decay curves of electrons, holes, and the sum of electrons and holes in $SrTiO_3$. The number of electrons and holes are calculated in the absence and presence of electron-scavenger (or hole-scavenger). The solid lines show the sum of $[e^-]$ and $[h^+]$, and the dotted lines show each of $[e^-]$ and $[h^+]$.

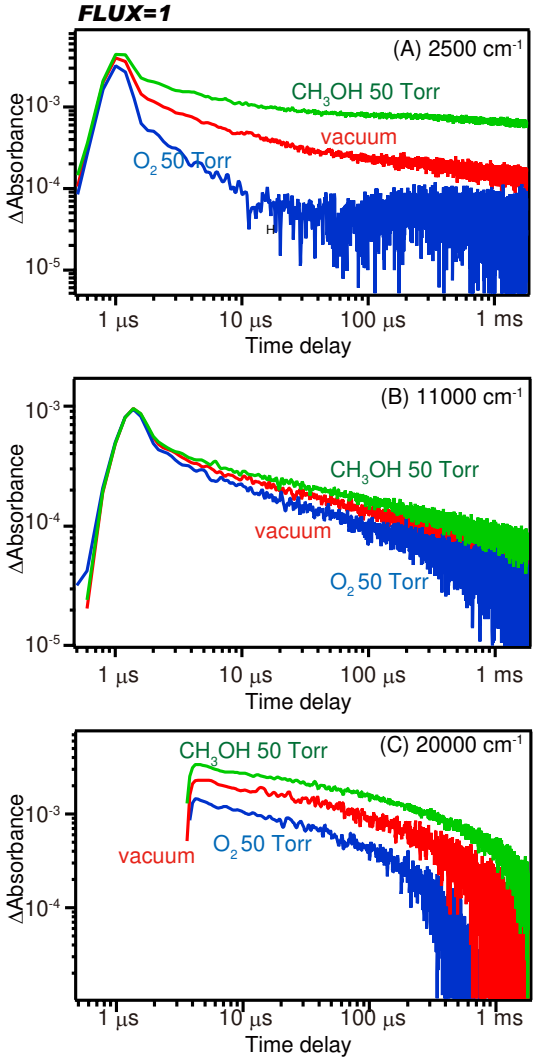

Fig. 6 Decay curves of transient absorption of flux-treated $SrTiO_3$ powder (FLUX=1) irradiated by 355 nm laser pulses (0.5 mJ per pulse at 0.2 Hz). The decay curves were measured at 2500 cm^{-1} (A), 11000 cm^{-1} (B), and 20000 cm^{-1} (C) in vacuum, 50 Torr O_2, and CH_3OH.

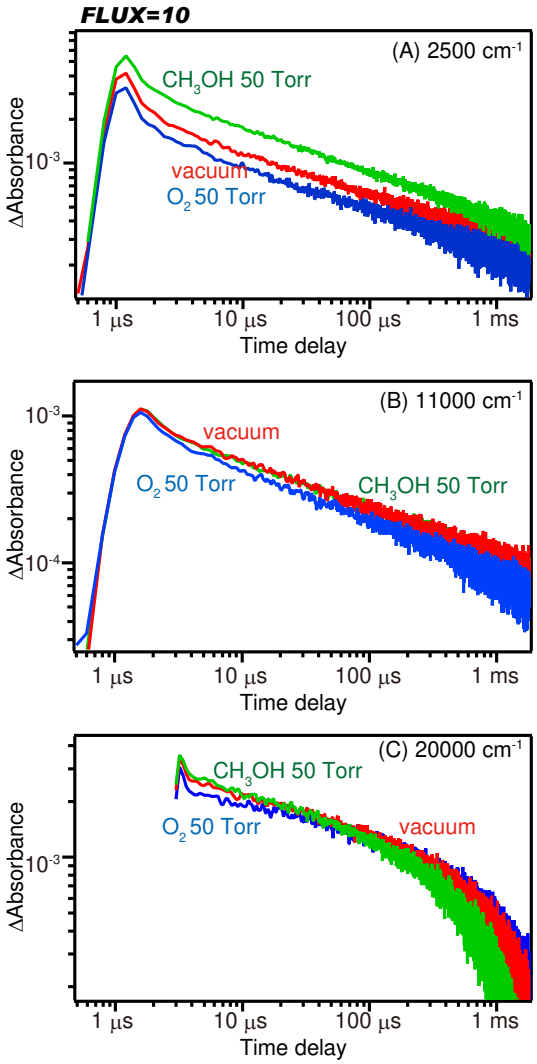

Fig. 7 Decay curves of transient absorption of flux-treated $SrTiO_3$ powder (FLUX=10) irradiated by 355 nm laser pulses (0.5 mJ per pulse at 0.2 Hz). The decay curves were measured at 2500 cm^{-1} (A), 11000 cm^{-1} (B), and 20000 cm^{-1} (C), in vacuum, 50 Torr O_2, and CH_3OH.

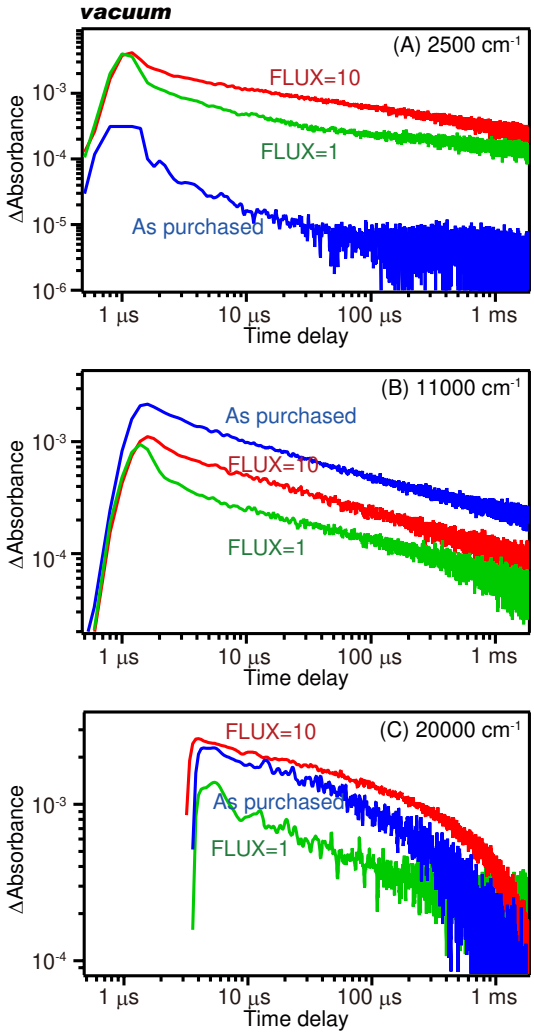

Fig. 8 Flux dependent decay curves of transient absorption of $SrTiO_3$ powder irradiated by 355 nm laser pulses (0.5 mJ per pulse at 0.2 Hz). The amount of flux was varied from $SrCl_2/SrTiO_3$=0 to 10. The decay curves were measured in a vacuum at 2500 cm^{-1} (A), 11000 cm^{-1} (B), and 20000 cm^{-1} (C).

Table. 1 Rates of H_2 and O_2 evolution from water splitting reaction on $Rh_xCr_{2-x}O_3$-loaded $SrTiO_3$, BET surface area, and elemental analysis of flux-treated samples.

FLUX	Activity(μmol/h)		FWHM of (110) peak	BET Surface area	[Sr]/[Ti]	2[Al]/([Sr]+[Ti])
($SrCl_2$/STO)	H_2	O_2		$m^2\ g^{-1}$	%	%
0	<1	<1	0.107	3.6	1.09	0.04
0.01	1	1	0.083	-	1.01	0.20
0.1	6	6	0.058	<0.3	1.02	0.19
1	40	21	0.061	0.5	1.00	0.18
5	470	240	0.064	0.8	-	-
10	450	240	0.066	0.9	0.98	0.31